J|A|C|S ARTICLES

Published on Web 04/29/2009

pH- and Photo-Switched Release of Guest Molecules from Mesoporous Silica Supports

Elena Aznar,[†,‡,§] Ma Dolores Marcos,[*,†,‡,§] Ramón Martínez-Máñez,[*,†,‡,§] Félix Sancenón,[†,‡,§] Juan Soto,[†,‡,§] Pedro Amorós,[*,||] and Carmen Guillem[||]

Instituto de Reconocimiento Molecular y Desarrollo Tecnológico, Centro Mixto Universidad Politécnica de Valencia - Universidad de Valencia, Spain, Departamento de Química. Universidad Politécnica de Valencia. Camino de Vera s/n 46022, Valencia, Spain, and CIBER de Bioingeniería, Biomateriales y Nanomedicina (CIBER-BBN), Institut de Ciència del Materials (ICMUV), Universitat de València, P.O. Box 2085, E-46071 València, Spain

Received December 23, 2008; E-mail: mmarcos@qim.upv.es; rmaez@qim.upv.es; pedro.amoros@uv.es

Abstract: This paper proposes a new nanoscopic molecular movable gate-like functional hybrid system consisting of nanoscopic MCM-41-based material functionalized onto pore outlets with a saccharide derivative capable of interacting with boronic acid functionalized gold nanoparticles (AuNPs) acting as nanoscopic caps. The gating mechanism involves the reversible reaction between polyalcohols and boronic acids to form boronate esters. Functionalized AuNPs thus act as a suitable nanoscopic cap via the reversible formation of the corresponding boroester bonds with the saccharide derivative anchored on the external surface of the mesoporous silica-based solid. The developed platform operates in aqueous solution and can be triggered by two simple external stimuli such as pH changes or light. The hydrolysis of the boroester bond takes place at pH 3, which results in rapid delivery of the safranine cargo from the pore voids into the aqueous solution. However, at pH 5 the pores are capped with nanoparticles and the delivery is strongly inhibited. The kinetics of the delivery was studied at pH = 3, assuming a simple diffusion process and that the kinetics of guest release from the pore voids of the hybrid material can be explained by the Higuchi model. It is possible to deliver the cargo in small portions by carrying out on−off aperture cycles via changing the pH from 3 to 5. AuNPs also open the possibility of employing light as a suitable stimulus for release procedures using the AuNPs' capacity for raising their temperature locally by absorption of laser light. The plasmonic heating using a Nd:YAG laser at 1064 nm results in the cleavage of the boronic ester linkage that anchors the nanoparticles to the surface of the mesoporous silica-based material, allowing the release of the entrapped guests. Further studies also demonstrated that it is possible to fine-tune the amount of cargo delivered by simply controlling the laser irradiation opening the possibility to designing laser-induced pulsatile release supports.

Introduction

The distinctive characteristics of functionalized mesoporous silica supports such as high homogeneous porosity, inertness, thermal stability, the presence of tunable pore sizes with a diameter of ca. 2−10 nm, homogeneous pore distribution, and the possibility to easily functionalize the external (or internal) surface makes these scaffoldings ideal for hosting functional guest molecules. Additionally, the possibility of incorporating in the external surface functional groups able to open or close at will or including capping molecules provides advanced control release applications. In fact, the unique architecture of such solids, containing parallel pores with two unique openings, makes it possible to design systems able to achieve zero release, which can be fully opened using external physical or chemical stimuli. Based on these concepts, systems functionalized with switchable molecules able to release confined guests as required or to admit molecular species to (or through) certain sites have been reported. Although such gating properties have also been reported on surfaces, in membranes[1] and certain porous systems,[2] the examples derived from the use of MCM-41-type siliceous solids are especially attractive because of the properties of the mesoporous materials (vide ante).[3] In this

† Instituto de Reconocimiento Molecular y Desarrollo Tecnológico.
‡ Departamento de Química. Universidad Politécnica de Valencia.
§ CIBER de Bioingeniería, Biomateriales y Nanomedicina (CIBER-BBN).
|| Institut de Ciència del Materials. Universitat de València.

(1) See for instance: (a) Jung, Y.; Bayley, H.; Movileanu, L. *J. Am. Chem. Soc.* **2006**, *128*, 15332–15340. (b) Joseph, S.; Mashl, R. J.; Jakobsson, E.; Aluru, N. R. *Nano Lett.* **2003**, *3*, 1399–1403. (c) Jeong, B.; Gutowska, A. *Trends Biotechnol.* **2002**, *20*, 305–311. (d) Ito, T.; Hioki, T.; Yamaguchi, T.; Shinbo, T.; Nakao, S.; Kimura, S. *J. Am. Chem. Soc.* **2002**, *124*, 7840–7846. (e) Rusell, T. P. *Science* **2002**, *297*, 964–967. (f) Ding, Z. L.; Fong, R. B.; Long, C. J.; Stayton, P. S.; Hoffman, A. S. *Nature (London)* **2001**, *411*, 59–62. (g) Galaev, I. Y.; Mattiasson, B. *Trends Biotechnol.* **1999**, *17*, 335–340. (h) Okano, T.; Bae, Y. H.; Jacobs, H.; Kim, S. W. *J. Controlled Release* **1990**, *11*, 255–265. (i) Irie, M. *Adv. Polym. Sci.* **1993**, *110*, 49–65. (j) Irie, M.; Misumi, Y.; Tanaka, T. *Polymer* **1993**, *34*, 4531–4535. (k) Sugawara, M.; Kojima, K.; Sazawa, H.; Umezawa, Y. *Anal. Chem.* **1987**, *59*, 2842–2846.

(2) Of special relevance is the development of artificial channels; see for instance. :(a) Yamaguchi, T.; Ito, T.; Sato, T.; Sginbo, T.; Nakao, S. *J. Am. Chem. Soc.* **1999**, *121*, 4078–4079. (b) Berger, J.; Reist, M.; Mayer, J. M.; Felt, O.; Peppas, N. A.; Gurny, R. *Eur. J. Pharm. Biopharm.* **2004**, *57*, 19–34.

 © 2009 American Chemical Society

context, photochemically, electrochemically, and ionically controlled gate-like elements have been incorporated into 3D MCM-41 scaffolds via tethering molecular or supramolecular gating ensembles on the pore outlets of the mesopores. In a "proof-of-the-concept" paper Fujiwara et al.[4] grafted photoresponsive coumarin onto the pore outlets of MCM-41 solids to develop a photochemically controlled molecular gate. Irradiation at $\lambda > 350$ nm resulted in the photodimerization of the coumarin core, which closed the pores by formation of a cyclobutane dimer, whereas the gate could be opened by using higher-energy irradiation at 250 nm to regenerate the coumarin monomer by photocleavage of the dimer. A similar gate-like ensemble was recently additionally functionalized with a light-driven "molecular stirrer" using the reversible isomerization of azobenzene groups.[5] The same authors have also reported a redox gate which is opened and closed by redox-controlled dimerization of thiol groups attached to the pore voids of an MCM-41-type material,[6] and Feng et al. have also reported a disulfide-reducing agent-responsive gate using a cross-linked polymeric network attached to the pore entrances.[7] Zink, Stoddart et al. designed supramolecular redox-controlled nanovalves containing grafted pseudorotaxanes and bistable rotaxanes in the pore outlets of mesostructured silica thin films.[8] The same authors have worked on systems that can be opened via an enzyme-mediated hydrolysis reaction[9] on a pH-driven mechanism using dialkylammonium threads[10] anchored to MCM-41 capped with dibenzo[24]crown-8 and on a nanovalve that relies on the ion−dipole interaction between curcubit[6]uril pseudorotaxanes and bisammonium stalks.[11] A pH-responsive gate on mesoporous materials based on a polypseudorotaxane has also been reported by Kim et al.,[12] and pH-driven gate-like elements have been reported by some of the present authors[13−15] and by Xiao et al.[16] via anchoring polyamines or carboxylic acids on mesoporous silica, respectively. Some of the present authors have also reported a bis-switching gate-like system controllable by light and chemical inputs using spiropyran moieties and carboxylate-containing dendrimers.[13b] Relevant examples on the regulation of the pore size in mesoporous systems have also been reported by using photoresponsive azobenzene-modified pore surfaces[17] or cleavable tails of suitable templates placed on the pore voids.[18] An automodulated release through mesoporous nanocompartment films has been described by Ji et al.[19] Skirtach et al. have employed multicompartment capsules for controlled mixing of two components.[20] Other notable gate-control examples reported by Lin et al. include mesoporous materials containing removable CdS[21] or magnetic[22] and gold nanoparticles[23] as blocking caps to prevent the leaching out of the cargo. These functional mesoporous supports have been applied to the controlled release of drugs, genes, biocides, dyes, and proteins and for the detection of certain target guests such as neurotransmitters, ATP, and fatty acids.[24,25] Most of these systems are designed for delivery assays and less commonly for sensing protocols.[26] Additionally, interesting examples containing gate-like systems have also been reported using nanotubes as suitable containers.[27]

From the research point of view, the study of the supramolecular functional aspects that arise from the covalent grafting of organic molecules onto preorganized or pre-existing stable

(3) (a) Kesge, C. T.; Leonowicz, M. E.; Roth, W. J.; Vartuli, J. C.; Beck, J. S. *Nature (London)* **1992**, *359*, 710–712. (b) Zhao, D.; Feng, J.; Huo, Q.; Melosh, N.; Fredrickson, G. H.; Chmelka, B. F.; Stucky, G. D. *Science* **1998**, *279*, 548–552. (c) Liu, Y.; Zhang, W.; Pinnavaia, T. J. *Angew. Chem., Int. Ed.* **2001**, *40*, 1255–1258. (d) Han, Y.; Li, D.; Zhao, L.; Xiao, F.-S. *Angew. Chem., Int. Ed.* **2003**, *42*, 3633–3638.

(4) (a) Mal, N. K.; Fujiwara, M.; Tanaka, Y. *Nature (London)* **2003**, *421*, 350–353. (b) Mal, N. K.; Fujiwara, M.; Tanaka, Y.; Taguchi, T.; Matsukata, M. *Chem. Mater.* **2003**, *15*, 2285–3394. (c) Zhu, Y.; Fujiwara, M. *Angew. Chem., Int. Ed.* **2007**, *46*, 2241–2244.

(5) (a) Lu, J.; Choi, E.; Tamanoi, F.; Zink, J. I. *Small* **2008**, *4*, 421–426. (b) Angelos, S.; Choi, E.; Vögtle, F.; De Cola, L.; Zink, J. I. *J. Phys. Chem. C.* **2007**, *111*, 6589–6592.

(6) Fujiwara, M.; Terashima, S.; Endo, Y.; Shiokawa, K.; Ohue, H. *Chem. Commun.* **2006**, 4635–4637.

(7) Liu, R.; Zhao, X.; Wu, T.; Feng, P. *J. Am. Chem. Soc.* **2008**, *130*, 14418–14419.

(8) (a) Hernandez, R.; Tseng, H.-R.; Wong, J. W.; Stoddart, J. F.; Zink, J. I. *J. Am. Chem. Soc.* **2004**, *126*, 3370–3371. (b) Nguyen, T. D.; Tseng, H.-R.; Celeste, P. C.; Flood, A. H.; Liu, Y.; Stoddart, J. F.; Zink, J. I. *Proc. Natl. Acad. Sci. U.S.A.* **2005**, *102*, 10029–10034. (c) Nguyen, T. D.; Liu, Y.; Saha, S.; Leung, K. C.-F.; Stoddart, J. F.; Zink, J. I. *J. Am. Chem. Soc.* **2007**, *129*, 626–634. (d) Angelos, S.; Johansson, E.; Stoddart, J. F.; Zink, J. I. *Adv. Funct. Mater.* **2007**, *17*, 2261–2271. (e) Saha, S.; Leung, K. C.-F.; Nguyen, T. D.; Stoddart, J. F.; Zink, J. I. *Adv. Funct. Mater.* **2007**, *17*, 685–693.

(9) Patel, K.; Angelos, S.; Dichtel, W. R.; Coskun, A.; Yang, Y. W.; Zink, J. I.; Stoddart, J. F. *J. Am. Chem. Soc.* **2008**, *130*, 2382–2383.

(10) Nguyen, T. D.; Leung, K. C.-F.; Liong, M.; Pentecost, C. D.; Stoddart, J. F.; Zink, J. I. *Org. Lett.* **2006**, *8*, 3363–3366.

(11) (a) Angelos, S.; Yang, Y.-W.; Patel, K.; Stoddart, J. F.; Zink, J. I. *Angew. Chem., Int. Ed.* **2008**, *47*, 2222–2226. (b) Nguyen, T. D.; Leung, K. C.-F.; Liong, M.; Liu, Y.; Stoddart, J. F.; Zink, J. I. *Adv. Funct. Mater.* **2007**, *17*, 2101–2110. (c) Leung, K. C.-F.; Nguyen, T. D.; Stoddart, J. F.; Zink, J. I. *Chem. Mater.* **2006**, *18*, 5919–5928.

(12) Park, C.; Oh, K.; Lee, S. C.; Kim, C. *Angew. Chem., Int. Ed.* **2007**, *46*, 1455–1457.

(13) (a) Casasús, R.; Marcos, M. D.; Martínez-Máñez, R.; Ros-Lis, J. V.; Soto, J.; Villaescusa, L. A.; Amorós, P.; Beltrán, D.; Guillem, C.; Latorre, J. *J. Am. Chem. Soc.* **2004**, *126*, 8612–8613. (b) Aznar, E.; Casasús, R.; García-Acosta, B.; Marcos, M. D.; Martínez-Máñez, R.; Sancenón, F.; Soto, J.; Amorós, P. *Adv. Mater.* **2007**, *19*, 2228–2231.

(14) Casasús, R.; Climent, E.; Marcos, M. D.; Martínez-Máñez, R.; Sancenón, F.; Soto, J.; Amorós, P.; Cano, J.; Ruiz, E. *J. Am. Chem. Soc.* **2008**, *130*, 1903–1917.

(15) Bernardos, A.; Aznar, E.; Coll, C.; Martínez-Máñez, R.; Barat, J. M.; Marcos, M. D.; Sancenón, F.; Soto, J. *J. Controlled Release* **2008**, *131*, 181–189.

(16) Yang, Q.; Wang, S.; Fan, P.; Wang, L.; Di, Y.; Lin, K.; Xiao, F.-S. *Chem. Mater.* **2005**, *17*, 5999–6003.

(17) Liu, N.; Dunphy, D.; Atanassov, P.; Bunge, S. D.; Chen, Z.; López, G. P.; Boyle, T. J.; Brinker, C. J. *Nano Lett.* **2004**, *4*, 551–554.

(18) Zhang, Q.; Ariga, K.; Okabe, A.; Aida, T. *J. Am. Chem. Soc.* **2004**, *126*, 988–989.

(19) Ji, Q.; Miyahara, M.; Hill, J. P.; Acharya, S.; Vinu, A.; Yoon, S. B.; Yu, J.-S.; Sakamoto, K.; Ariga, K. *J. Am. Chem. Soc.* **2008**, *130*, 2376–2377.

(20) See for instance: (a) Skirtach, A. G.; Antipov, A. A.; Shchukin, D. G.; Sukhorukov, G. B. *Langmuir* **2004**, *20*, 6988–6992. (b) Skirtach, A. G.; Dejugnat, C.; Braun, D.; Susha, A. S.; Rogach, A. L.; Parak, W. J.; Möhwald, H.; Sukhorukov, G. B. *Nano Lett.* **2005**, *5*, 1371–1377. (c) Skirtach, A. G.; Javier, A. M.; Kreft, O.; Köhler, K.; Alberola, A. P.; Möhwald, H.; Parak, W. J.; Sukhorukov, G. B. *Angew. Chem., Int. Ed.* **2006**, *45*, 4612–4617. (d) Kreft, O.; Skirtach, A. G.; Sukhorukov, G. B.; Möhwald, H. *Adv. Mater.* **2007**, *19*, 3142–3145.

(21) Lai, C.-Y.; Trewyn, B. G.; Jeftinija, D. M.; Jeftinija, K.; Xu, S.; Jeftinija, S.; Lin, V. S.-Y. *J. Am. Chem. Soc.* **2003**, *125*, 4451–4459.

(22) Giri, S.; Trewyn, B. G.; Stellmaker, M. P.; Lin, V. S.-Y. *Angew. Chem., Int. Ed.* **2005**, *44*, 5038–5044.

(23) Torney, F.; Trewyn, B. G.; Lin, V. S.-Y.; Wang, K. *Nat. Nanotechnol.* **2007**, *2*, 295–300.

(24) Radu, D. R.; Lai, C.-Y.; Jeftinija, K.; Rowe, E. W.; Jeftinija, S.; Lin, V. S.-Y. *J. Am. Chem. Soc.* **2004**, *126*, 13216–13217.

(25) (a) Trewyn, B. G.; Giri, S.; Slowing, I. I.; Lin, V. S.-Y. *Chem. Commun.* **2007**, 3236–3245. (b) Trewyn, B. G.; Slowing, I. I.; Giri, S.; Chen, H.-T.; Lin, V. S.-Y. *Acc. Chem. Res.* **2007**, *40*, 846–853. (c) Slowing, I. I.; Trewyn, B. G.; Giri, S.; Lin, V. S.-Y. *Adv. Funct. Mater.* **2007**, *17*, 1225–1236.

(26) (a) Casasús, R.; Aznar, E.; Marcos, M. D.; Martínez-Máñez, R.; Sancenón, F.; Soto, J.; Amorós, P. *Angew. Chem., Int. Ed.* **2006**, *45*, 6661–6664. (b) Coll, C.; Casasús, R.; Aznar, E.; Marcos, M. D.; Martínez-Máñez, R.; Sancenón, F.; Soto, J.; Amorós, P. *Chem. Commun.* **2007**, 1957–1959.

nanoscopic supports is a subject that we find particularly captivating.[28] However, in relation to gated systems, many reported examples still harbor disadvantages for their potential use in advanced applications. Typical limitations include no reversibility, no operational features in aqueous environments, the use of a unique stimulus for release applications, etc. Taking into account that examples that operate reversibly in response to two or more stimuli are still rare, we were particularly interested in developing systems showing delivery functions triggered by a least two different inputs and that additionally are able to display controlled release in a pure aqueous solution. We were also attracted by the possibility of developing delivery systems where cargo release could be controlled at will in small portions (controlled pulsatile release). In particular, and as a part of our interest in the use of inorganic supports for advanced applications,[29] we report here the design of a nanoscopic molecular movable gate-like functional hybrid system that can be controlled by both pH and NIR laser radiation. The nanoscopic MCM-41-based material was synthesized and grafted onto the pore outlets with a saccharide derivative capable of interacting with boronic acid functionalized gold nanoparticles that act as nanoscopic caps. The gating effect in water as a function of the pH and NIR laser radiation is studied via the controlled release of the dye safranine O from the pore voids to the bulk solution.

Results and Discussion

Design and Synthesis. For the design of the proposed controlled release scaffolding, two components were chosen, namely a suitable support and the responsive "gate-like" ensemble. As inorganic scaffolding we selected mesoporous materials of the MCM-41 family as a suitable inorganic matrix, due to its high homogeneous porosity, inertness, and ease of functionalization on its surface.[30] For the gating mechanism it was our aim to develop a platform that could operate in aqueous solution and that could be triggered by using two simple external stimuli such as pH changes or light (vide infra). We therefore focused our attention on the reversible reaction between polyalcohols and boronic acids to form boronate esters.[31] The polyalcohols were anchored on the external surface of the mesoporous material, whereas boronic acids were anchored on gold nanoparticles (AuNPs). Functionalized AuNPs were expected to act as a suitable nanoscopic cap via the formation of the corresponding boroester bonds with the saccharide derivative anchored on the external surface of the mesoporous silica-based solid. At the same time the use of AuNPs opens the possibility of employing light as a suitable stimulus for release procedures using the capacity of AuNPs for raising their temperature locally due to the absorption of laser light (vide infra).

With this aim, the mesoporous MCM-41 support was functionalized with a saccharide derivative. From the wide range of possibilities, the derivative *N*-(3-triethoxysilylpropyl)gluconamide as a simple and commercially available, yet suitable, open-chain molecular entity was selected and was anchored through covalent bonds on the pore outlets of an MCM-41 material. To study the functional open/close protocol, the dye Safranine O was loaded on the inner mesopores of the 3D organized MCM-41 solid.

As it has been reported, the inorganic 3D matrix, dye, and functional gating groups should be arranged in a programmed mode in the synthesis of the gating material. Thus, the solid matrix (MCM-41 type solids) must contain the cargo in the pores, whereas the molecular movable mechanism (in our case the polyalcohols) should ideally only be anchored on the outer surface (the pore outlets). To prepare this organized hybrid material (see Scheme 1), the mesoporous scaffold was first synthesized (see Experimental Section). The calcination of the mesostructured phase provided the starting solid, MCM-41. After removal of adsorbed water by azeotropic distillation, the safranine O dye was added to the suspension and stirred for 24 h with the aim of completely loading the pores of the MCM-41 scaffolding. An excess of *N*-(3-triethoxysilylpropyl)gluconamide (to yield **S1**) was then added, and the suspension was stirred for 5.5 h. During this time, the polyalcohol-silane derivative is maintained in the suspension, which still contains a high concentration of the dye to disfavor the diffusion of the latter from the pores to the solution. Anchoring of the organosilane is a rapid reaction, although it cannot be completely ruled out that some organosilane molecules will diffuse into the mesopores. The quick reaction of the organosilane with the siliceous surface and the presence of pores filled with the dye makes it feasible to obtain structures where the saccharide derivative is basically placed on the external surface of the mesoporous silica-based scaffolding. The final purple solid (**S1**) was filtered, washed with acetonitrile, and dried at 50 °C for 12 h. A similar two-step synthetic procedure has been used recently by other authors to develop responsive operational

(27) (a) Nednoor, P.; Chopra, N.; Gavalas, V.; Bachas, L. G.; Hinds, B. J. *Chem. Mater.* **2005**, *17*, 3595–3599. (b) Hillebrenner, H.; Buyukserin, F.; Kang, M.; Mota, M. O.; Stewart, J. D.; Martin, C. R. *J. Am. Chem. Soc.* **2006**, *128*, 4236–4237.

(28) (a) Descalzo, A. B.; Martínez-Máñez, R.; Sancenón, F.; Hoffmann, K.; Rurack, K. *Angew. Chem., Int. Ed.* **2006**, *45*, 5924–5948. (b) Ariga, K.; Vinu, A.; Hill, J. P.; Mori, T. *Coord. Chem. Rev.* **2007**, *251*, 2562–2591. (c) Martínez-Máñez, R.; Sancenón, F. *Coord. Chem. Rev.* **2006**, *250*, 3081–3093. (d) Ariga, K.; Hill, J. P.; Lee, M. V.; Vinu, A.; Charvet, R.; Acharya, S. *Sci. Technol. Adv. Mater.* **2008**, *9*, 104–109.

(29) (a) Climent, E.; Calero, P.; Marcos, M. D.; Martínez-Máñez, R.; Sancenón, F.; Soto, J. *Chem.—Eur. J.* **2009**, *15*, 1816–1820. (b) Ros-Lis, J. V.; Casasús, R.; Comes, M.; Coll, C.; Marcos, M. D.; Martínez-Máñez, R.; Sancenón, F.; Soto, J.; Amorós, P.; El Haskouri, J.; Garró, N.; Rurack, K. *Chem.—Eur. J.* **2008**, *14*, 8267–8278. (c) Comes, M.; Marcos, M. D.; Martínez-Máñez, R.; Sancenón, F.; Soto, J.; Villaescusa, L. A.; Amorós, P. *Chem. Commun.* **2008**, 3639–3641. (d) Calero, P.; Aznar, E.; Lloris, J. M.; Marcos, M. D.; Martínez-Máñez, R.; Ros-Lis, J. V.; Soto, J.; Sancenón, F. *Chem. Commun* **2008**, 1668–1670. (e) Descalzo, A. B.; Marcos, M. D.; Monte, C.; Martínez-Máñez, R.; Rurack, K. *J. Mater. Chem.* **2007**, *17*, 4716–4723. (f) Coll, C.; Martínez-Máñez, R.; Marcos, M. D.; Sancenón, F.; Soto, J. *Angew. Chem., Int. Ed.* **2007**, *46*, 1675–1678. (g) Comes, M.; Marcos, M. D.; Martínez-Máñez, R.; Millán, M. C.; Ros-Lis, J. V.; Sancenón, F.; Soto, J.; Villaescusa, L. A. *Chem.—Eur. J.* **2006**, *12*, 2162–2170. (h) Basurto, S.; Torroba, T.; Comes, M.; Martínez-Máñez, R.; Sancenón, F.; Villaescusa, L. A.; Amorós, P. *Org. Lett.* **2005**, *7*, 5469–5472. (i) Descalzo, A. B.; Marcos, M. D.; Martínez-Máñez, R.; Soto, J.; Beltrán, D.; Amorós, P. *J. Mater. Chem.* **2005**, *15*, 2721–2731. (j) Comes, M.; Rodríguez-López, G.; Marcos, M. D.; Martínez-Máñez, R.; Sancenón, F.; Soto, J.; Villaescusa, L. A. *Angew. Chem., Int. Ed.* **2005**, *44*, 2918–2922. (k) Comes, M.; Marcos, M. D.; Martínez-Máñez, R.; Sancenón, F.; Soto, J.; Villaescusa, L. A.; Amorós, P.; Beltrán, D. *Adv. Mater.* **2004**, *16*, 1783–1786. (l) Rodríguez-López, G.; Marcos, M. D.; Martínez-Máñez, R.; Sancenón, F.; Soto, J.; Villaescusa, L. A.; Beltrán, D.; Amorós, P. *Chem. Commun.* **2004**, 2198–2199.

(30) (a) Beck, J. S.; Vartuli, J. C.; Roth, W. J.; Leonowicz, M. E.; Kresge, C. T.; Schmitt, K. D.; Chu, C. T.-W; Olson, D. H.; Sheppard, E. W.; McCullen, S. B.; Higgins, J. B.; Schlenker, J. L. *J. Am. Chem. Soc.* **1992**, *114*, 10834–10843. (b) Wright, A. P.; Davis, M. E. *Chem. Rev.* **2002**, *102*, 3589–3614. (c) Kickelbick, G. *Angew. Chem., Int. Ed.* **2004**, *43*, 3102–3104. (d) Stein, A. *Adv. Mater.* **2003**, *15*, 763–775.

(31) See for instance: (a) James, T. D.; Shinkai, S. *Top. Curr. Chem.* **2002**, *18*, 159–200. (b) Wang, W.; Gao, X.; Wang, B. *Curr. Org. Chem.* **2002**, *6*, 1285–1317.

Scheme 1. Preparation of Solids **S1** and **S2** and the pH and Laser Light Triggered Release of the Entrapped Guest (the Dye Safranine O)

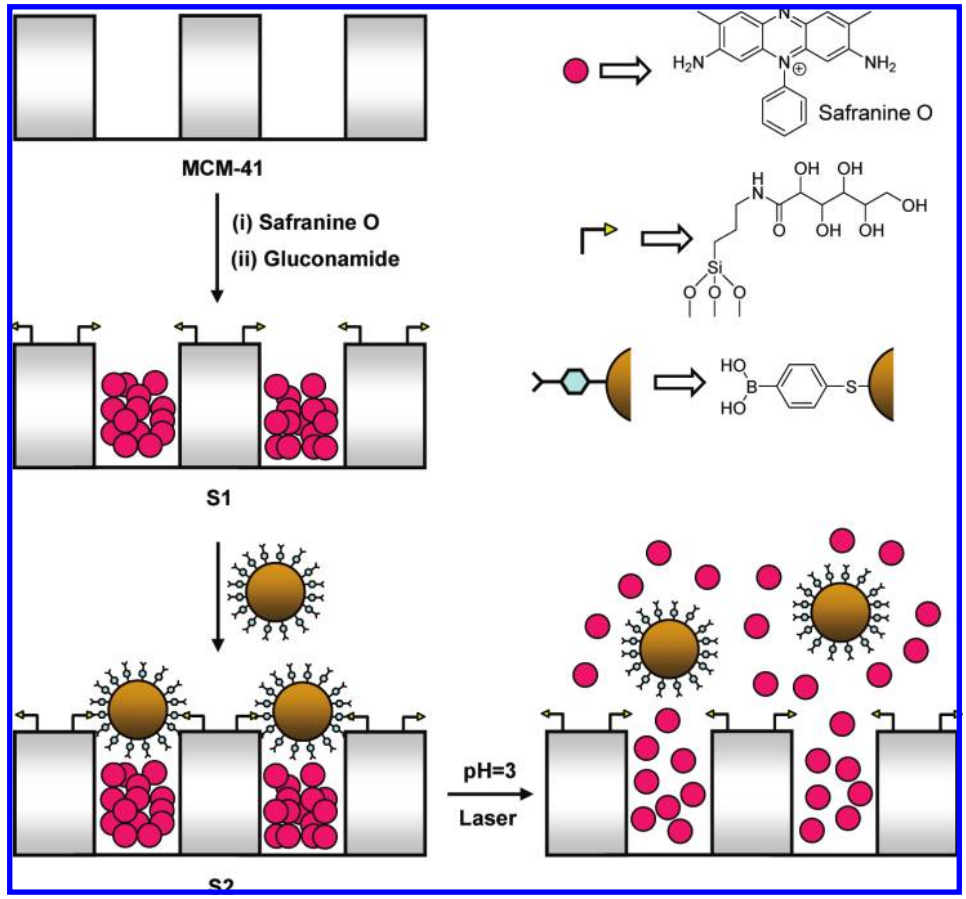

gating structures containing a certain cargo in the pores and suitable switchable ensembles on the pore outlets.[13,14,16,17]

The boronic acid capped gold nanoparticles (**B-AuNPs**) were obtained by the Brust method via the addition of a freshly prepared aqueous solution of sodium borohydride to a methanolic solution of hydrogen tetrachloroaurate(III) and 4-mercaptophenylboronic acid with vigorous stirring. The solvent was then removed under reduced pressure, and the dark-brown residue was washed thoroughly, first with diethyl ether and then with deionized water to finally obtain the functionalized **B-AuNPs** with an average size of 3 nm. AuNPs in the 5−40 nm range are known to show strong surface plasmon resonance at green wavelengths (λ in the range 520−540 nm), whereas if the nanoparticles are smaller than 5 nm the plasmon resonance band is broadened due to surface scattering,[32] resulting in the prepared **B-AuNPs** being brown in color.

The functional open/close protocol of the nanoscopic gate-like ensemble was tested by measuring the release of the safranine O dye loaded on the inner mesopores of the 3D organized MCM-41 solid. The dye was chosen because of its relatively high molar absorptivity, high solubility, and stability in water in a wide pH range. The gate-like effect can then be straightforwardly studied via the delivery of the dye from the pore voids to the aqueous solution through the visible band of the safranine O centered at 521 nm in the water phase. Scheme 1 shows a representation of the prepared solids and the controlled release protocol.

(32) Daniel, M. C.; Astruc, D. *Chem. Rev.* **2004**, *104*, 293–346.

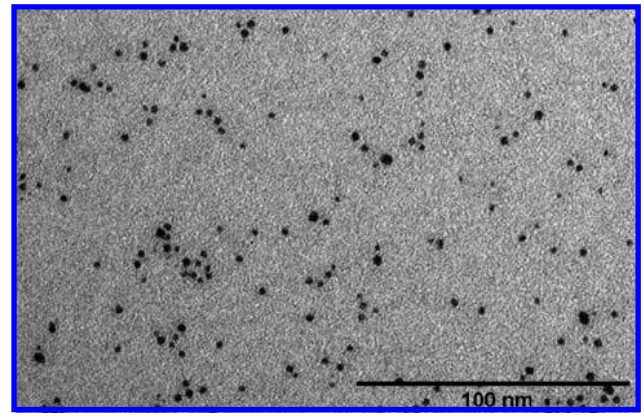

Figure 1. Representative TEM photograph of the functionalized **B-AuNPs**.

Characterization of the Boronic Acid Functionalizated Gold Nanoparticles. Figure 1 shows a representative Transmission Electron Microscopy (TEM) photograph of the boronic acid functionalized gold nanoparticles (**B-AuNPs**). The size and size distribution of the **B-AuNPs** were also studied with a size particle analyzer, and the results can be seen in Figure 2. An average size of 3.1 nm, and a remarkably narrow size distribution can be observed. The XRD of the functionalized nanoparticles (see Figure 3) shows typical reflections for a cubic array of Au atoms that can be indexed as (111), (200), and (220) Bragg peaks with an a_0 cell parameter of 4.1 Å (d_{111} spacing of 2.35 Å). The quantification of the content of the organic molecule was accomplished by thermogravimetric studies and

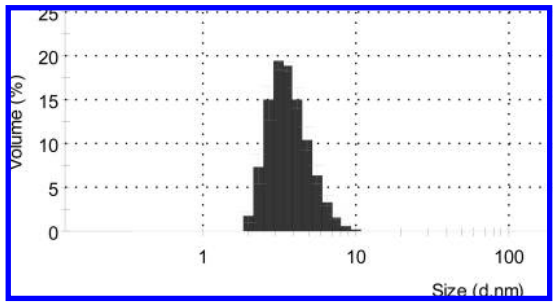

Figure 2. Size distribution of **B-AuNPs**.

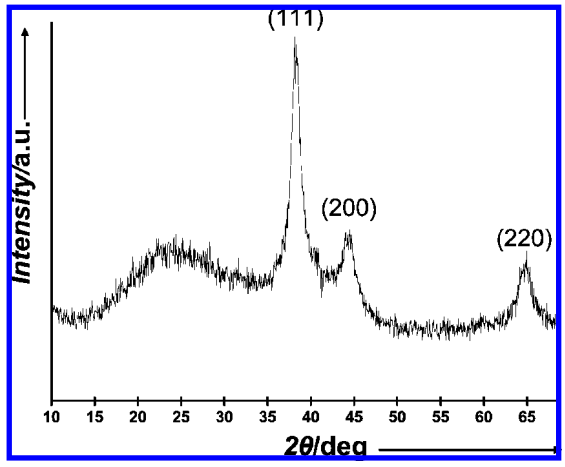

Figure 3. Powder X-ray patterns of the of the gold nanoparticles functionalized with boronic acid **B-AuNPs**. The broad peak at ca. 25° is due to the scattering of the glass amorphous support.

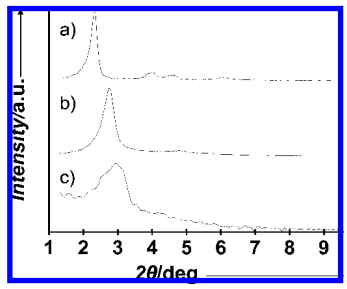

Figure 4. Powder X-ray patterns of the solids (a) MCM-41 as-synthesized, (b) MCM-41 calcined, and (c) the final **S1** solid containing the dye and the anchored gluconamide.

elemental and EDX analysis. Typical boronic acid content in the **B-AuNPs** is 16.43% wt, which gives ca. 190 boronic acid molecules per particle.

Characterization of S1. Figure 4 shows powder X-ray patterns of the solids MCM-41 as-synthesized, MCM-41 calcined, and the final **S1** solid containing the dye and the anchored polyalcohols. The XRD of siliceous MCM-41 as-synthesized shows four low-angle reflections typical of a hexagonal array that can be indexed as (100), (110), (200), and (210) Bragg peaks with an a_0 cell parameter of 43.7 Å (d_{100} spacing of 37.8 Å). A significant displacement of the (100) peak in the XRD powder of the MCM-41 calcined sample is clearly appreciated in the (b) curve corresponding to an approximate cell contraction of 7.3 Å. This displacement and the broadening of the (110), (200) peaks are typically related to condensation of silanols during the calcination step. In Figure 4, the (c) curve corresponds to the **S1** XRD pattern. In this case, the loss of the (110) and (200)

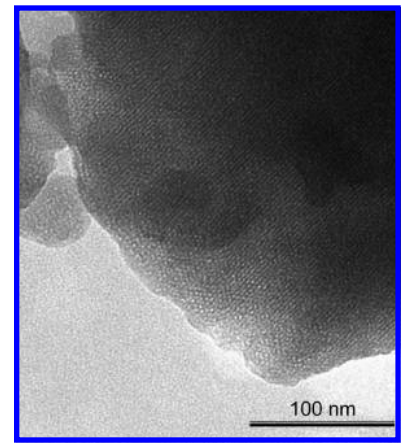

Figure 5. TEM image of the solid **S1** showing the typical hexagonal porosity of the MCM-41 matrix.

reflections is observed, most likely related to a loss of contrast due to the filling of the pore voids with the safranine O dye. Nevertheless, the value and intensity of the d_{100} peak in this pattern are strong evidence that the loading process with the dye and the further functionalization with polyalcohols have not damaged the mesoporous 3D MCM-41 scaffolding. The mesoporous structure in the final functionalized solids is also observed from the TEM studies (see Figure 5), in which the typical hexagonal porosity of the MCM-41 matrix can be seen.

The evolution of the porosity with the inclusion of dye molecules and the functionalization of the mesopore outlets can be appreciated in the isotherms displayed in Figure 6. The N_2 adsorption−desorption isotherms of the MCM-41 parent calcined material shows a typical type IV curve of surfactant-assisted mesoporous silicas with a single, strong, and sharp adsorption step at intermediate relative partial pressure values around 0.3. This feature is associated with the nitrogen condensation inside the mesopores by capillarity. The application of the BET model resulted in a high value for the specific surface of 1201.8 m^2/g. On the other hand, the BJH model applied on the adsorption branch of the isotherms leads to a pore diameter of 2.33 nm. The absence of a hysteresis loop in this interval of P/P_0, as well as the narrow BJH pore size distribution, suggests the existence of uniform cylindrical channels throughout the material (according to XRD and TEM). From XRD and porosimetry, a value for the *wall thickness* of 1.31 nm can be calculated as the difference between a_0 (3.64 nm) and pore size (2.33 nm). The wall thickness value corresponds approximately to the intermesopore silica range at the particle surface where the polyalcohols are anchored.

After dye loading and the mesopore outlets are functionalized (solid **S1**), a significant decrease in the N_2 volume adsorbed is observed according to the N_2 adsorption−desorption isotherm shown in Figure 6b. In fact, solid **S1** presents flat curves when compared (at the same scale) to those of the MCM-41 parent material, thus indicating a significant pore blocking and the subsequent absence of appreciable porosity. This is an expected result bearing in mind that solid **S1** contains polyalcohol-functionalized external surfaces and a high content of Safranine O dye filling the pores. In spite of this extremely low porosity, when the curve is *y*-enlarged a typical IV type isotherm, similar to those of MCM-41, appears. Hence, a single adsorption step in the 0.1−0.3 P/P_0 range is observed. This residual mesoporosity could be attributed to a certain inhomogeneity of the polyalcohols at the pore entrances, this leading to a small

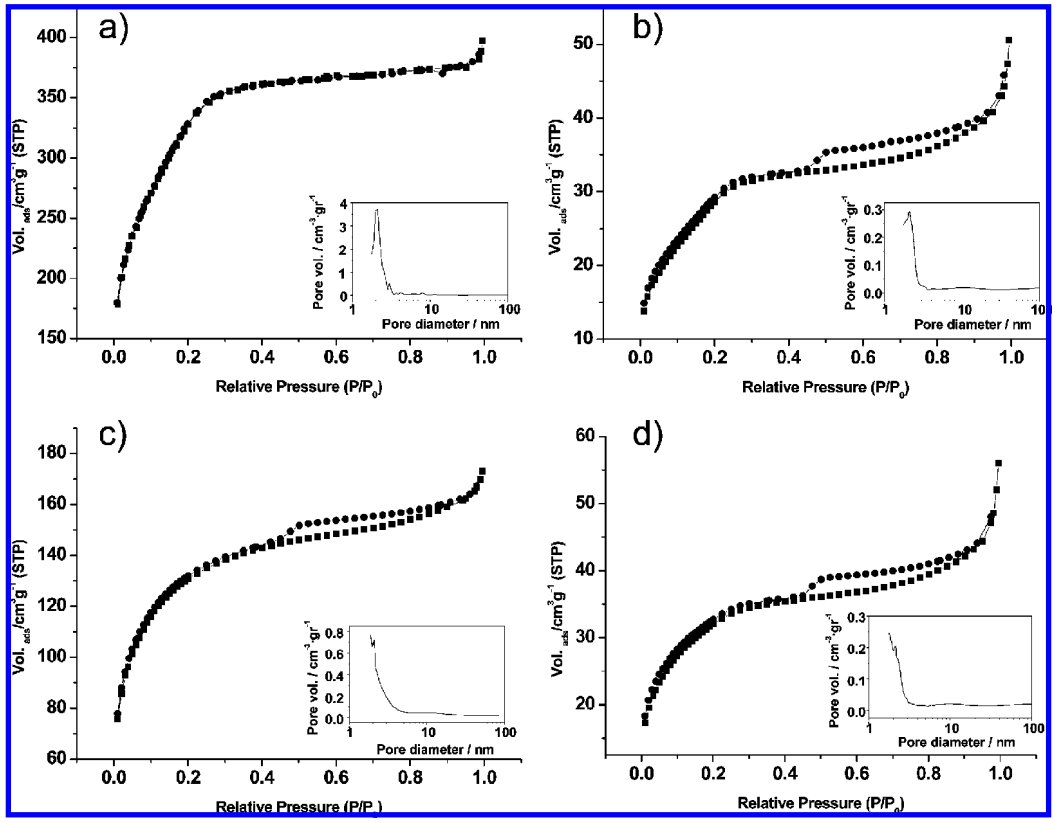

Figure 6. Nitrogen adsorption−desorption isotherms for (a) **MCM-41** mesoporous material, (b) **S1**, (c) **S1-1**, and (d) **S2**. Insets: Pore size distribution of each material.

proportion of nonfunctionalized and then accessible pores. After this first feature in the isotherm, at medium and higher P/P_0 values the curve shows a continuous increase and separates from an expected type IV isotherm. In fact, the curve shape in this pressure range (similar to type II isotherms) and the presence of a clear H_2-type hysteresis loop is consistent with a multilayer adsorption process characteristic of layered pore-free samples. Thinking on the dry conditions achieved during the sample evacuation prior to the analysis, this adsorption could be attributed to a textural-like porosity among particles probably generated during the evacuation process and encouraged by the polyalcohol moieties anchored onto the external surface of the lamellar microparticles, as can be observed by TEM. In this case, the hysteresis loop observed must be consequence of stacking defects due to the lack of the homogeneous size of the layered particles. Significant decreases in the BET area (from 1201.8 to 107.8 m^2/g) and the BJH pore volume (see Table 1) occur from MCM-41 to sample **S1**. On the contrary, practically similar pore sizes have been determined: 2.33 and 2.20 nm for samples MCM-41 and **S1**, respectively. This feature suggests that the residual porosity remaining in sample **S1** could be attributed to a low proportion of unaltered mesopores. Hence, the low porosity, together with the typical mesoporous-like X-ray powder diffraction profile (showing a characteristic intense but extremely weak peak at low angle values) and the TEM images for **S1** (see Figures 4 and 5), provides direct evidence of the high efficiency of the dye loading.

Additionally, to study in detail the independent effect that the anchoring of the polyalcohols groups has on the pore accessibility, a new solid was prepared from a sample of solid **S1** that was allowed to deliver the most of the Safranine O dye. This new solid **S1-1** still contains a residual color, most likely due to strongly adsorbed dye onto the pores that could not be delivered under the experimental conditions. Isothermal N_2 adsorption−desorption curves of **S1-1** show isotherms somehow similar in shape to those of solid **S1**. However, both the BET surface area (469.7 m^2/g) and the BJH pore volume (see Table 1) show a large increase after the Safranine O dye evolution. These values clearly indicate that although some of the surface has been lost probably due to the polyalcohol functionalization and the presence of a certain proportion of undelivered dye, a significant amount of porosity (~50% when compared to the parent MCM-41) can be recovered after the colorant has been delivered. In fact, we have to bear in mind that the dry conditions achieved during the sample evacuation prior to the adsorption−desorption analysis may produce significant dehydration around the polyalcohol groups anchored at the pore entrances, leading to a collapse of the anchors and the subsequent (at least) partial pore blocking.

Table 1. BET Specific Surface Values, Pore Volume, and Pore Size Calculated from the N_2 Adsorption−Desorption Isotherms for the Materials Used in This Work

sample	S_{BET}/ m^2/g	pore size[a]/ nm	BJH pore[b]/ nm	total pore volume[c]/ cm^3/g	pore volume ($P/P_0 < 0.6$)[d]/ cm^3/g	pore volume ($P/P_0 > 0.6$)[e]/ cm^3/g
MCM-41	1201.8	2.09	2.33	0.50	0.45	0.05
S1	107.8	2.11	2.20	0.07	0.05	0.02
S1-1	469.7	2.15	2.17	0.17	0.14	0.03
S2	116.9	2.15	2.23	0.07	0.04	0.03

[a] Pore size at the peak maximum in the pore size distribution. [b] Pore size estimated by using the BJH model applied on the adsorption branch of the isotherm. [c] Total pore volume according to the BJH model. [d] Pore volume for $P/P_0 < 0.6$, which can be associated to the surfactant generated mesopores. [e] Pore volume for $P/P_0 > 0.6$, which can be associated to the textural porosity.

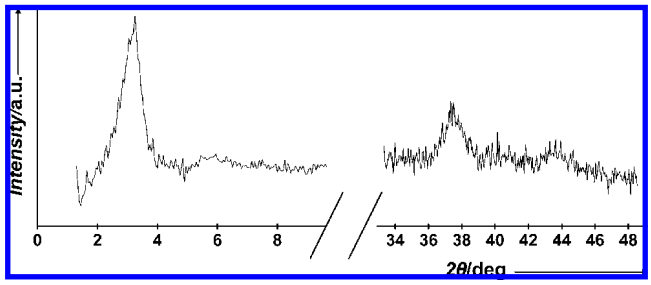

Figure 7. Powder X-ray patterns of the solid **S2** (a) from $2\theta = 1.3°$ to 10°, (b) from $2\theta = 34°$ to 50°.

In relation to the calculation of the pore diameter for the **S1-1** sample, the isotherm curvature at low pressure suggests the presence of supermicropores (average pore size for this solid lower than 2.0 nm) in the border between meso- and micropores. The proximity to the low limit measurement regime of the equipment avoids an accurate pore size determination. In any case, the curve shape and the achieved value are consistent with a partial and inhomogeneous pore blocking due to the collapse of the polyalcohol groups at the pore entrances and the presence of some undelivered colorant. The H_2-type hysteresis loop related to a certain textural porosity above-mentioned for the sample **S1** is preserved after dye delivery. The obtained results on **S1-1** strongly suggest that even in the "dry state" necessary for N_2 adsorption−desorption measurements, some aperture at the pore openings may still remain in the solid **S1-1**.

Quantification of the content of the glucose derivative and the safranine O dye was accomplished by thermogravimetric studies, elemental analysis, and EDX analysis. Typical dye and saccharide contents in the final solid **S1** are 10 and 5% wt, respectively.

Characterization of the S2 Hybrid Material. As will be shown below, the interaction of the solid **S1** with the functionalized **B-AuNPs** provide a system showing zero release in water at neutral pH. To characterize this ensemble, we prepared solid **S2** by adding **S1** to a suspension of the **B-AuNPs** in ethanol. After several washing processes, the solid **S2** was obtained. The successful incorporation of the **B-AuNPs** in the **S1** matrix was confirmed by various methods. Figure 7 shows the powder X-ray diffraction pattern of the **S2** solid in the $1.3° < 2\theta < 10°$ range, which confirms the presence of the mesoporous structure. Figure 7 also displays the X-ray diffraction in the $34° < 2\theta < 50°$ range, which shows similar diffraction peaks to those observed for the **B-AuNPs** alone (see Figure 3), confirming the presence of the functionalized gold nanoparticles on the final **S2** material. As expected, the N_2 adsorption/desorption isotherms of the gold nanoparticle capped mesoporous **S2** material displayed an isotherm very similar to that shown by sample **S1**, i.e., with relatively flat curves when compared to MCM-41 and a low residual porosity probably associated with some inhomogeneous pore outlets functionalization (BET surface area of 116.9 $m^2 g^{-1}$; pore volume = 0.07 cm^3/g; pore size = 2.23 nm). The remaining (majority) mesopores are completely blocked due to the presence of dye molecules (filling the pores) and gold nanoparticles (at the pore entrances). Additionally, the presence of the boronic acid capped AuNPs in the final solid **S2** is also confirmed from TEM analysis (see Figure 8) that shows the characteristic mesoporous channels as alternate black and white stripes. Additionally, the **B-AuNPs** are clearly visible as dark zones on the outside of the mesopores (indicated in the figure by arrows). These zones are not observed in the corresponding solid **S1**, which is not capped with **B-AuNPs**.

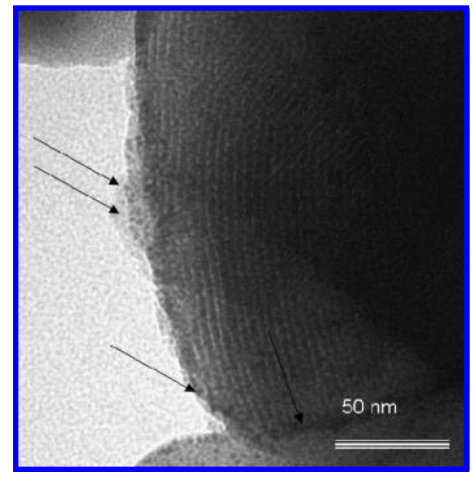

Figure 8. TEM image of the solid **S2** showing the mesostructure. The arrows point to gold nanoparticles.

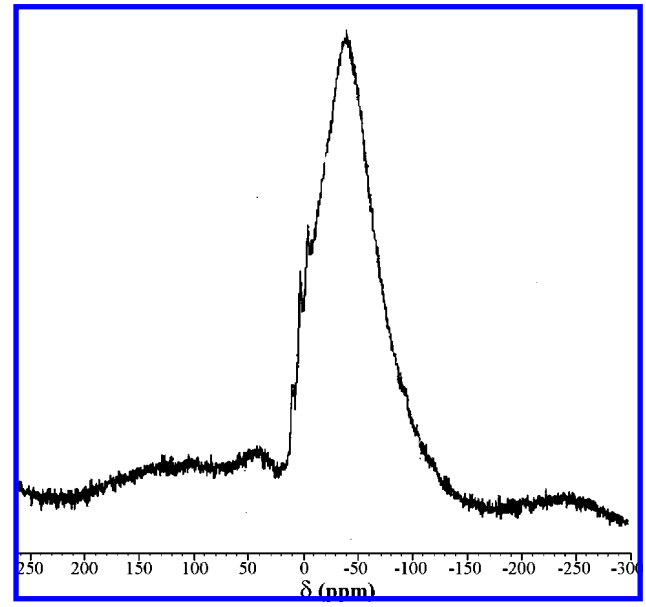

Figure 9. ^{11}B MAS NMR spectrum of **S2**.

To complete the characterization of the gold nanoparticle-capped mesoporous **S2** material, boron NMR studies were carried out. The ^{11}B MAS NMR spectrum of sample **S2** is shown in Figure 9. An intense and broad band centered at −37 ppm with some overlapped signals at chemical shift values in the 10−15 ppm range was observed. The absence of intense signals around 20 ppm (only a weak broad signal was found in this range) indicates the absence of trigonal sp^2-hybridized neutral B-species[33] and strongly suggests that the boron atoms are in a tetra- or pseudotetrahedral sp^3-hybridized form.[34] Additionally, according to the bibliography, the intense and broad band centered at −38 ppm and the signals between 10 and −15 ppm could be assigned to anionic terminal boronic acid groups and boronic esters, respectively.[35] The variety of possible bond connections between B atoms and sugars through one, two, or even three oxygen atoms (including the possibility to connect

(33) Kroeker, S.; Stebbins, J. F. *Inorg. Chem.* **2001**, *40*, 6239–6246.
(34) Baldwin, J. E.; Claridge, T. D. W.; Derome, A. E.; Smith, B. D.; Twyman, M.; Waley, S. G. *Chem. Commun.* **1991**, 573–574.
(35) Nakazawa, I.; Suda, S.; Masuda, M.; Asai, M.; Shimizu, T. *Chem. Commun.* **2000**, 881–882.

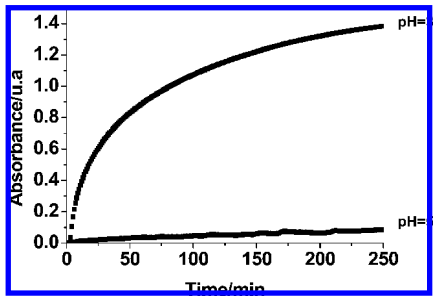

Figure 10. Release profiles of Safranine O in water from solid **S2** at pH 3 and 5.

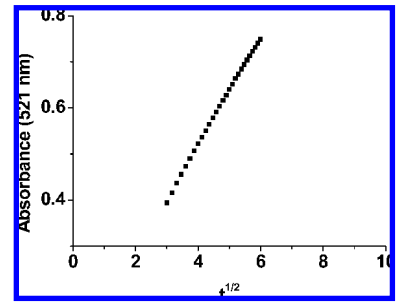

Figure 11. Linear relationship of the experimental absorbance at 521 nm (dye delivered) versus the square root of the time (t) for the delivery of safranine O from the pores of solid **S1** at pH 3.

different closely anchored sugars)[36] could be the reason for observing different signals.

After confirming from the NMR data the formation of boronic ester groups and before starting to detail the controlled release studies on the AuNPs capped solid **S2**, it is important to note that one crucial subject in controlled release materials using mesoporous supports is if the guest molecules are located inside the pores or in the interparticle porosity. A look to the porosity measurements on solids MCM-41, **S1**, **S1-1**, and **S2** might shed some light on this subject (see Table 1). The MCM-41 starting material shows a large pore volume (0.45 $cm^3\ g^{-1}$) due to the surfactant generated mesopores and a certain interparticle textural porosity (0.05 $cm^3\ g^{-1}$). When this scaffolding is filled with the dye and functionalized with the saccharide to prepare **S1** or is further capped with the **B-AuNPs** to synthesize **S2**, the mesopore volume decreases remarkably to 0.05−0.04 $cm^3\ g^{-1}$, whereas when the dye is released from **S1** to give **S1-1**, the pore volume due to the mesopore increases significantly (0.14 $cm^3\ g^{-1}$). Yet for all the solids the interparticle porosity remains similar in value (between 0.02−0.05 $cm^3\ g^{-1}$). Although it cannot be completely ruled out that some dye could be placed in the interparticle textural porosity, the porosimetry data strongly suggest that most of the guest molecules really exist in the mesopores and most of the dye is also delivered from the pore space.

Functional pH-Driven Controlled Release. The effectiveness of the gate-like ensemble with changes in the proton concentration (pH-driven "nanogates") was studied with the hybrid material **S2**. A pH range was employed to effect the controlled release of the safranine O dye from the pore voids of the mesoporous silica-based system into the aqueous solution. We give here the results obtained at pH 3 and 5, at which a differentiable switching behavior was clearly observed.

In a typical dye-release experiment, 10 mg of **S2** were placed in a plastic cartridge, and then water (25 mL) at a certain pH was recirculated through the sample for a certain amount of time. The increase in the absorption band at 521 nm in the aqueous solution indicated a corresponding leak of safranine O from the pores. A very clear and highly effective pH-controllable gating effect can be seen in Figure 10, which plots the release profiles of the dye for solid **S2** at pH 3 and 5. The figure shows that at pH 5 there is no dye delivery, while at pH 3 there is considerable leakage of the safranine O dye; i.e., "the gate-like" ensemble is fully open.

The nondelivery at pH 5 (a similar behavior is found at neutral pH) has to be interpreted in terms of the formation of the corresponding boronic esters during the synthesis of **S2** by reaction between the **B-AuNPs** and the saccharide derivative anchored at the pore voids of the mesoporous **S1** support. Thus, when **S2** is placed in water the pores are capped with the nanoparticles and the delivery of the cargo is strongly inhibited. In fact, the results shown in Figure 10 indicate that most of the pore openings on **S2** were effectively blocked by the boronic acid decorated gold nanoparticles.

As stated above, the boronate ester bonds between the mesoporous solid and the **B-AuNPs** are labile and can be cleaved by changes in the pH via the hydrolysis of the bonds. This effect is clearly observed in Figure 10, which shows how at pH 3 there is quick delivery of the safranine cargo from the pore voids to the aqueous solution. 82% of the total safranine was relased in a period of 2 h.

At pH 3 the kinetics of the delivery was studied, assuming that a simple diffusion process occurs and that the kinetics of guest release from the pore voids of the mesoporous **S1** material could be explained by the Higuchi model.[37] This model suggests that if the release of the cargo is diffusion-controlled, then the release should be dependent on the square root of time. The model states that the amount of guest release, Q_t, per unit of exposed area at time t can then be described by the simple equation

$$Q_t = k_H \sqrt{t} \qquad (1)$$

where k_H is the release rate constant for the Higuchi model. This equation has for instance been widely and satisfactorily applied for related porous silica systems used for the noncontrolled release of drugs.[38] We applied this model to the delivery of the Safranine O dye at pH 3. A good linear fitting was observed (see Figure 11), indicating that the delivery of the dye from the pores of solid **S1** is basically a diffusive process. This means that, at pH 3, when there is no interaction between the saccharide derivatives and the functionalized nanoparticles, the tethered saccharides behave like threads anchored on the external surface, which allows a simple diffusive mass transport of the dye from the pore voids to the bulk solution. This scheme contrasts with that found for pH 5, where the cargo release is strongly inhibited and no kinetic studies could be carried out. Thus, for instance, **S2** exhibited less than 4% release of the

(36) Nicholls, M. P.; Paul, P. K. C. *Org. Biomol. Chem.* **2004**, *2*, 1434–1441.

(37) (a) Higuchi, T. *J. Pharm. Sci.* **1961**, *50*, 874–875. (b) Higuchi, T. *J. Pharm. Sci.* **1963**, *52*, 1145–1149.

(38) See for instance: (a) Vallet-Regí, M.; Balas, F.; Arcos, D. *Angew. Chem., Int. Ed.* **2007**, *46*, 7548–7558. (b) Vallet-Regí, M.; Rámila, A.; del Real, R. P.; Pérez-Pariente, J. *Chem. Mater.* **2001**, *13*, 308–311. (c) Muñoz, B.; Rámila, A.; Pérez-Pariente, J.; Díaz, I.; Vallet-Regí, M. *Chem. Mater.* **2003**, *15*, 500–503. (d) Anderson, J.; Rosenholm, J.; Areva, S.; Linden, M. *Chem. Mater.* **2004**, *16*, 4160–4167.

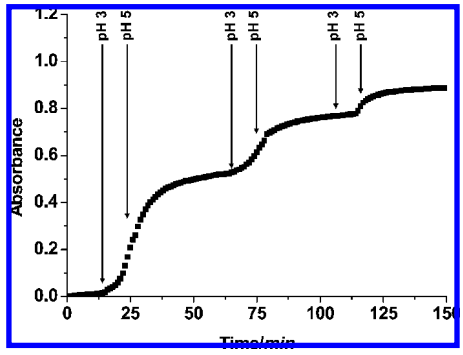

Figure 12. Partial guest release from solid **S2** as function of pH variations.

safranine dye in the aqueous solution at pH 5 over a period of 2 h.

We were particularly concerned with the possibility that the observed effect might not have been caused by the formation of boronate esters between the saccharide-functionalized surface of the mesoporous silica-based scaffolding and the boronic acid functionalized gold nanoparticles, but due to some simple interaction of the **B-AuNPs** with the silica surface. To eliminate this possibility, solid **S3** was prepared. **S3** consists of an MCM-41 support loaded with the dye but not functionalized with the sugar derivative in the pore outlets. Dye delivery studies using **S3** in water at pH 3 and 5 in the presence of **B-AuNPs** were carried out, but no gating effect was observed; i.e., the delivery process is very rapid and similar at both pH values. We were also concerned with the possibility that the pH-controlled effect might have been due to a possible change in the conformation of the anchored sacharides, as a function of the proton concentration. To eliminate this possibility, additional delivery studies were also carried out with solid **S1** without the presence of **B-AuNPs**. In this case no effect in the cargo delivery was observed when the experiments are carried out at pH 3 or pH 5 and very similar quick release curves were found. Both experiments indicate that the pH-controllable gate-like functional effect is only observed for the solid containing saccharide-functionalized mesoporous surfaces when it is in the presence of boronic acid functionalized gold nanoparticles. These results strongly suggest that the opening/closing of the pores is most likely related to the formation of boronate esters at neutral pH and the hydrolysis of these bonds under acidic conditions.

pH Triggered Reversible Open−Close Protocol. In the design of controlled release systems it is not only important to achieve the complete cargo delivery as required, but for some applications it might also be necessary to deliver the entrapped guests in small portions (controlled pulsatile release). To achieve this goal the open−close protocol used for controlling the release of the mesopore-entrapped guest must be switched "on" and "off" at will. Bearing in mind that the formation of boronate esters is in principle reversible, studies directed toward the possibility of delivering the cargo on **S1** in portions were carried out. The effect achieved is shown in Figure 12.

For the experiment, 10 mg of **S2** were placed in a plastic cartridge, and then water (25 mL) at a certain pH was recirculated through the sample for a certain time. The starting pH was 5, at which the delivery of the cargo was inhibited. The pH was then suddenly changed to 3 by addition of acid. This is indicated in the figure by an arrow. This change in pH triggered a rapid release of the mesopore-entrapped safranine as a consequence of the rupture of the boroester bonds. After 10 min the pH was again set to 5 (see the arrow in the figure). This change in pH inhibits the release of the entrapped dye. The inhibition process however is slower than when the delivery is triggered. This is somehow expected because complete inhibition would not be observed until all the unanchored **B-AuNPs** in the solution have been reacted with the saccharide-derivative functionalized mesoporous silica-based support. At time 60 min, pH 3 was selected again and further delivery of the entrapped dye was observed until pH 5 was again set, inhibiting the release of the dye. This on−off switching of the delivery was repeated once more. The release of the dye is reduced in each on−off sequence because the amount of dye to be delivered from the pores to the solution is reduced in each cycle (see Figure 12). The results demonstrated that the opening/closing protocol is reversible and that a partial cargo delivery or the delivery of the cargo in small portions can be controlled at will.

Plasmon-Enhanced Heating Opening Protocol. AuNPs are among the most intensely studied nanoparticles due not only to their physical and chemical properties but also to well-known supramolecular and recognition effects.[29] However in this section we focused on one of the properties of metal nanoparticles related to their characteristic multiparameter-dependent surface plasmon resonance and their capacity for raising their temperature locally by absorption of laser light.[39] Plasmon resonance excitation in AuNPs produces photothermal effects from the nonradiative relaxation of the optically excited conduction electrons, whose energy is dissipated as heat into the surrounding medium. The photothermal properties of AuNPs have been applied to different fields such as photothermal contrast agents,[40] optothermally controlled drug release,[20] and localized hyperthermal therapy.[41]

These observations suggest that a suitable opening protocol of the pores, when using AuNPs as caps, can be the use of light as a switching mechanism. Plasmonic heating could cause cleavage of the boronic ester linkage that anchors **B-AuNPs** to the surface of the mesoporous silica-based **S2** material. To test this possibility a Quantel Brilliant/Brilliant B Q-Switched Nd:YAG laser at 1064 nm (226 mJ) was used to irradiate the sample with a pulse duration of 4.3 ns. The experiments were carried out using 2 mg of **S2** suspended in 5 mL of water at pH 7 (no dye release) and then irradiated with 5 pulses at 1064 nm. The suspension was stirred during the pulse irradiation and then for a further 10 min to allow the dye to diffuse from the pores to the solution. The suspension was then filtered, and the clear red coloration of the aqueous solution was observed, indicating dye release from the irradied mesoporous silica-based **S2** material. Figure 13 shows the visible spectrum of the **S2** solutions before and after the laser irradiation process. A remarkably simple and highly effective light-induced release can be observed.

(39) (a) Pitsillides, C. M.; Joe, E. K.; Wei, X.; Anderson, R. R.; Lin, C. P. *Biophys. J.* **2003**, *84*, 4023–4032. (b) Hu, M.; Hartland, G. V. *J. Phys. Chem. B* **2002**, *106*, 7029–7033. (c) Link, S.; El-Sayed, M. A. *Int. Rev. Phys. Chem.* **2000**, *19*, 409–453. (d) Burda, C.; Chen, X.; Narayanan, R.; El-Sayed, M. A. *Chem. Rev.* **2005**, *105*, 1025–1102.
(40) Cognet, L.; Berciaud, S.; Lasne, D.; Lounis, B. *Anal. Chem.* **2008**, *80*, 2288–2294.
(41) See for instance: (a) Huang, X.; Jain, P.; El-Sayed, I. H.; El-Sayed, M. A. *Lasers Med. Sci.* **2007**, *23*, 217–228. (b) Huang, X.; Jain, P. K.; El-Sayed, I. H.; El-Sayed, M. A. *Nanomedicine* **2007**, *2*, 681–693. (c) Jain, P. K.; El-Sayed, I. H.; El-Sayed, M. A. *Nano Today* **2007**, *2*, 18–29.

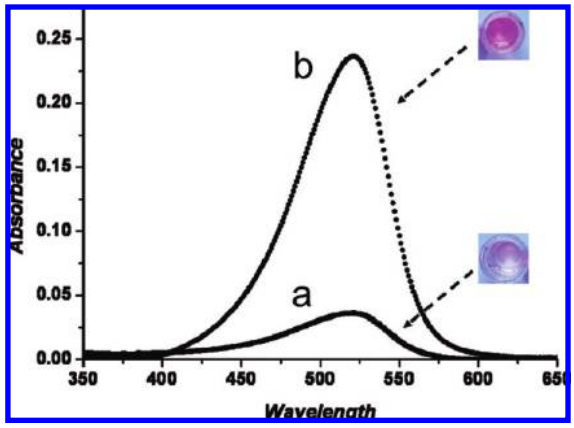

Figure 13. UV−vis spectra of solutions of solid **S2** (a) at pH 7 and (b) after 5 pulses irradiation with a Nd:YAG laser at 1064 nm.

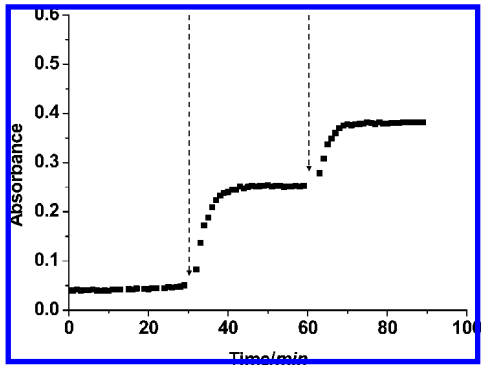

Figure 14. Partial guest release from solid **S2** controlled by the irradiation with the laser light.

Pulsatile Plasmon-Resonance-Triggered Open Protocol. Above it has been shown that it is possible to control at will a partial cargo delivery in small portions by changing the pH. In this section we were interested in studying whether it is also possible to deliver the cargo in a pulsatile mode by controlling the irradiation of the sample with the Nd:YAG laser. Bearing in mind that the rupture of the boronic ester linkage that anchors **B-AuNPs** to the surface of the mesoporous silica-based **S2** material would in principle depend on the laser energy that will reach the sample, we believed that it might be possible to control the amount of released cargo by controlling the number of laser pulses. Studies directed toward this possibility were carried out. For the experiment, 10 mg of **S2** were placed in a cuvette in water at pH 7. Under these conditions no significant delivery was observed. Then the sample was, after 30 min, irradiated with 5 pulses of a Nd:YAG laser at 1064 nm (226 mJ). This is indicated in Figure 14 by an arrow. The irradiation triggered a rapid release of the entrapped safranine as a consequence of the rupture of the boroester bonds. After ca. 10 min the absorbance at the solution remains constant indicating that no more dye release occurs. At time 60 min, the sample was again irradiated with 5 pulses of the Nd:YAG laser that again triggers the delivery of more entrapped dye. As it was found in the pH triggered protocol (see Figure 12), in this plasmon-resonance triggered release, the delivery of the dye is reduced in each sequence because the dye that remains in the pores is reduced progressively. In summary, the studies demonstrated that it is also possible to fine-tune the amount of cargo delivered by simply controlling the laser irradiation, opening the possibility of designing laser-induced pulsatile release supports.

Finally, to further study the relation between light and pH release, more experiments were carried out. The laser induced release was studied also at pH 5, and similar results to those found in Figure 14 for pH 7 were observed. A similar experiment to that shown in Figure 10 (pH induced release) was carried out in the dark to determine if visible light could have some effect in the pH triggered delivery; however no effect was found. These experiments suggest that only the potent laser light is able to induce delivery and that the light induced delivery is pH-independent.

Conclusions

The development of systems for releasing guest molecules from mesoporous silica supports using molecular and supramolecular concepts is currently taking chemistry to the forefront of nanoscience. It is possible to obtain simple and very effective guest release control using polyalcohol entities anchored onto mesoporous materials and boronic acid functionalized gold nanoparticles as effective caps. Both pH-controlled and NIR light-controlled delivery effects have been observed to occur in pure water. In relation to the pH-controlled delivery, the release of the cargo is inhibited at pH 5, whereas there is rapid release of the guest molecule from the mesoporous silica scaffolding at pH 3. The pH-controlled release is reversible, and the entrapped guests can be delivered in installments by simple changes in the pH. The pH-controlled "open−close" mechanism is associated with the reversible formation of boroesters between alcohol groups and boronic acid functionalized nanoparticles (closed-gate) and their quick and easy hydrolysis (open-gate). At the same time the use of AuNPs opens the way to employing light as a suitable stimulus for release procedures. This is related to the ability of AuNPs to raise their temperature locally by absorbing laser light. Plasmonic heating results in cleavage of the boronic ester linkage that anchors the nanoparticles to the surface of the mesoporous silica-based material, allowing the release of the cargo. A fine-tune of the amount of cargo delivered by simply controlling the laser irradiation is also possible. Both pH and light are easy-to-use external stimuli and appealing methods of releasing entrapped guests that could be used to develop new controlled delivery systems for a wide range of different applications. The possibility of using these stimuli for delivering cargo in small portions also opens the possibility of designing stimuli-induced pulsatile release supports.

Experimental Section

Synthesis. General Methods. XRD, TG analysis, elemental analysis, EDX microscopy, N_2 adsorption−desorption, UV−visible spectroscopy, NMR, and particle size analysis techniques were employed to characterize the materials obtained. X-ray measurements were performed on a Bruker AXS D8 Advance using Cu Kα radiation. Thermogravimetric analyses were carried out on a TGA/SDTA 851e Mettler Toledo balance, using an oxidant atmosphere (Air, 80 mL/min) with a heating program consisting of a dynamic segment (10 °C per minute) from 298 to 1273 K followed by a 1273 K isothermal segment for 30 min. EDX analyses were performed on a Jeol JSM 6300 operated at 20 kV. TEM images were obtained with a 100 kV Philips CM10 microscope. N_2 adsorption−desorption isotherms were recorded on a Micromeritics ASAP2010 automated sorption analyzer. The samples were degassed at 70 °C under vacuum overnight. The specific surface areas were calculated from the adsorption data in the low pressure range using the BET model. Pore size was determined following the BJH method. UV−visible spectroscopy was carried out with a Lambda 35 UV/vis spectrometer (Perkin-Elmer Instruments). The

size of the **B-AuNPs** was studied with a size particle analyzer Malvern Zetasizer ZS. A ^{11}B MAS NMR spectrum was recorded on a Varian Unity 300 spectrometer operating at 128.3 MHz and using a magic angle spinning speed of 4.0 kHz. ^{11}B chemical shifts were referenced to boric acid.

The reagents employed in the synthesis of **S1**, tetraethyl orthosilicate (TEOS), *n*-cetyltrimethylammonium bromide (CTAB), and triethanolamine ($TEAH_3$) were purchased from Fluka. Sodium hydroxide (NaOH) and dry acetonitrile were purchased from Scharlau. The organosilane *N*-(3-triethoxysilylpropyl)gluconamide was purchased from ABCR, and the dye safranine O was provided by Aldrich. All the reagents were used as received without further purification.

The reactives employed in the synthesis of **B-AuNPs**, hydrogen tetrachloroaurate(III), 4-mercaptophenylboronic acid, and sodium borohydride were purchased from Aldrich. Methanol and diethyl ether were obtained from Sharlau, and acetic acid was purchased from Merck. All the reagents were used as received without further purification.

Synthesis of MCM-41. The synthesis strategy we used to prepare MCM-41 silicas is an application of the so-called "atrane route", a simple preparative technique based on the use of triethanolamine-related ($TEAH_3$) ligands (i.e., in general "atranes" and silatranes for the silicon-containing complexes) as hydrolytic inorganic precursors and surfactants as porogen species. The molar ratio of the reagents in the mother liquor was fixed to 8 $TEAH_3$:2 TEOS: 0.52 CTAB:0.5 NaOH:180 H_2O for the synthesis of MCM-41. In a typical synthesis leading to MCM-41 pure silica, 4.68 g of CTAB (cetyltrimethylammonium bromide) were added at 118 °C to a solution of $TEAH_3$ (25,79 mL) containing 0.045 mol of a silatrane derivative (e.g., in the form of Si(TEA)($TEAH_2$), TEA is the fully deprotonated ligand). 80 mL of water were then added with vigorous stirring at 70 °C. After a few minutes, a white suspension was formed. This mixture was aged at room temperature overnight. The resulting powder was collected by filtration and washed with water. Finally, the solid was dried at 70 °C for 12 h. To prepare the final porous material, the as-synthesized solid was calcined at 550 °C using oxidant atmosphere for 5 h in order to remove the template phase. The presence of pores of uniform size lined with silanol groups confers potential interest of these materials as hosts for a variety of guest chemical species.

Synthesis of S1. In a typical synthesis, 1.5 g of the MCM-41 solid were suspended in 55 mL of anhydrous acetonitrile and heated in a Dean−Stark trap to remove the adsorbed water in the mesoporous support via azeotropic distillation. Then safranine O dye (0.42 g, 1.2 mmol) was added to the suspension and stirred for 24 h at room temperature with the aim of loading the pores of the MCM-41 scaffolding. After this loading procedure, the reactive *N*-(3-triethoxysilylpropyl)gluconamide (50% in ethanol, 1.575 mL, 1.97 mmol) was added and the suspension was stirred for 5.5 h. The purple solid (**S1**) was filtered, washed with acetonitrile, and dried at 50 °C for 12 h. This synthetic procedure assures a preferential grafting of the sugar derivative at the pore outlets rather than inside the pore walls, which are basically filled by the safranine O dye.

Synthesis of B-AuNPs. The boronic acid functionalizated nanoparticles (**B-AuNPs**) were obtained following a modification of the Brust method carried out in a single-phase system.[42] Hydrogen tetrachloroaurate(III) (30% wt. in dilute hydrochloric acid, 0.305 mL, 0.38 mmol) and 4-mercaptophenylboronic acid (0.029 gr., 0.19 mmol) were dissolved in methanol (75 mL). To prevent deprotonation of the boronic acid, acetic acid (1.5 mL) was added. 15 mL of freshly prepared 0.4 mol dm^{-3} aqueous sodium borohydride solution were then carefully added in small portions of ca. 1 mL with vigorous stirring. The solution turned brown immediately, indicating the formation of gold nanoclusters in the size range of ~3.1 nm. After further stirring for 30 min the solvent was removed under reduced pressure without exceeding the temperature 50 °C. The dark-brown residue was washed thoroughly with diethyl ether to remove excess 4-mercaptophenylboronic acid. After evaporation of the diethyl ether the material was also thoroughly washed with deionized water to remove borates and acetates and finally dried to obtain the dark-brown solid **B-AuNPs**. The **B-AuNPs** can be slowly (1 week) resuspended in ethanol absolute, helped occasionally by ultrasonication.

Synthesis of S2. To obtain the hybrid solid that functions as a molecular gate, a portion of 500 mg of **S1** was added to a suspension of 5 mg of **B-AuNPs** in 125 mL of ethanol basified with 0.2 mL of 2 M NaOH and stirred for 16 h. The resulting solid **S2** was then washed with ethanol and dried.

Synthesis of S3. For the sake of comparison, 500 mg of **S1** were washed with ethanol to obtain the solid **S3** with a similar amount of safranine O as **S2**.

Dye Release Studies. 25 mL of aqueous solutions with different pH values were used for evaluating the gate-like effect via studying dye release from the pore voids of the polyalcohol-functionalized materials. A cartridge loaded with 10 mg of the corresponding solid (**S2** and the related blank **S3**) was inserted into a flux cell, and the system was then filled with the corresponding solution (water at a certain pH) and maintained in circulation for 250 min. The delivery of the safranine O dye from the pore voids to the aqueous solution was monitored via the band of the dye centered at 521 nm.

Acknowledgment. The authors wish to express their gratitude to the Spanish Ministerio de Ciencia y Tecnología (Projects CTQ2006-15456-C04-01 and CTQ2006-15456-C04-03) for their support. E.A. is grateful to the Spanish Ministerio de Ciencia e Innovación for an FPU grant.

JA810011P

(42) Brust, M.; Fink, J.; Bethell, D.; Schiffrin, D. J.; Kiely, C. *J. Chem. Soc., Chem. Commun.* **1995**, 1655–1656.